Asymptotic Reflection of a Self-Propelled Particle from a Boundary Wall

Tomoyuki Miyaji *† Robert Sinclair‡

May 11, 2023

Abstract

Exact expressions for the relationship between angles of incidence and reflection from a boundary wall in nonlinear dissipative particle models are extremely rare. Here, we study a particle model of a camphor disk floating on water in a low speed limit, for which the model was derived. We begin with a very rough and inaccurate approximation, based in part on a Hamiltonian limit of the model, and then, using symmetry arguments supported by a series of experiments, show that this rough approximation can likely be repaired by introducing a factor dependent upon model parameters, then extract the full parameter dependence of this factor, and finally conjecture a simple and exact asymptotic relationship between the angles of incidence and reflection. There are reasons to believe that this asymptotic relationship may be universal for such models in their corresponding limits.

Keywords: Billiards, self-propelled particle, nonspecular reflection, asymptotic expansion.

1 Introduction

The movements of spatially localized structures in nonlinear dissipative systems have a significant economic and societal impact, tropical cyclones [1] being a prominent example, and it is not surprising that many fundamental discoveries in the theory of dynamical systems were motivated by attempts to understand aspects of atmospheric phenomena [14]. The discovery of mobile spatially localized structures in nonlinear dissipative systems describing diverse chemical and physical systems (e.g. [11], [10], [24], [23], [4], [28], [9], [26] and [18]) has only increased the importance of understanding how these structures move and

*Department of Mathematics, Kyoto University, Kyoto 606-8502, Japan.
ORCID iD: 0000-0002-2599-5409
†email: tmiyaji@math.kyoto-u.ac.jp
‡Hosei University, Tokyo, Japan.
ORCID iD: 0000-0002-9646-4322

react to various influences in their environment. It is becoming ever clearer that progress in understanding aspects of any one such system does tend to benefit research in the area as a whole, and our work has been undertaken in this spirit.

We will focus on the fundamental process of reflection of a single moving spatially localized structure from a boundary wall. While one has a natural tendency to expect the formula "angle of reflection equals angle of incidence" to apply, it is useful to reflect upon the fact that even a rubber ball may behave otherwise [8]. The point is that even a single particle interacting with a boundary can exhibit nontrivial and complicated phenomena. In our case, we will be focusing on a specific kind of spatially localized structure in a low speed limit, a subtle case in which the structures sense but do not actually touch the boundary wall, and therefore a phenomenon which is different from the familiar behavior of bouncing balls.

To be more specific, we will study reflection from a boundary wall of a camphor disk moving along the surface of water [18]. Previous mathematical modeling suggests that it behaves somewhat like a billiard ball but with a nonspecular reflection rule, where the angle of reflection is greater than that of incidence (see [3] and [5]), a phenomenon which has also been observed in numerical simulations of a model of a cavity soliton billiard system [23] and both theoretically and experimentally for walking droplets [25].

Accordingly, trajectories are quite different from those of standard mathematical billiards. This nonspecular reflection rule, for a single camphor disk moving very slowly on water, is studied in this paper.

Our study is similar in spirit to those of reflections from boundaries of spiral waves, which are extended dissipative structures in excitable media having a clearly identifiable center. In the most superficial sense, one may imagine these as looking like the tropical cyclones mentioned above, but see [32] for an accurate description. Under appropriate conditions, the centers of these spiral waves move in straight lines [21, 12] unless perturbed by interactions with other spirals [32] or boundaries. Reflection from a boundary wall is also nonspecular [12], and in some cases spirals are annihilated rather than reflected [21]. Despite the significant differences between the behaviors of these spiral waves and camphor disks floating on water, studies of asymptotic properties of reflection from a boundary have also been undertaken for spiral waves [13].

We study a system of ordinary differential equations (ODEs), which is derived from a planar reaction-diffusion model of a camphor disk on the surface of water [3] (see [10] and [3] for the reaction-diffusion model). The rest state and stationary motion of the camphor disk are modeled by a stationary spot solution and a traveling spot solution, respectively. As a parameter of the system (δ) varies, the stationary spot changes its stability at some threshold. In a sufficiently small parameter interval around the threshold, it is possible to reduce the dynamics of stationary and traveling spots to ODEs which describe the center of the disk and deformation of the profile from the stationary spot/particle. It is known that, despite the unavoidable simplifications associated with their construction, particle models of the kind we will consider here are surprisingly faithful representations of the experimentally observed motions of camphor disks

on water [2].

Once a functional relation $\theta_{\mathrm{ref}} = F(\theta_{\mathrm{inc}})$ between the angle of incidence θ_{inc} and that of reflection θ_{ref} is given, one can consider a discrete-time model to investigate the trajectory of a particle in a bounded region, assuming that the billiard table is extremely large relative to the size of the particle. Theoretical and numerical studies suggest that F is continuously differentiable on $[0, \pi/2]$, monotone increasing, and that it satisfies $F(\theta) \geq \theta$ for $\theta \in [0, \pi/2]$, where equality holds for $\theta = 0, \pi/2$. Under these conditions, it has been proven that a unique square-shaped periodic orbit exists on a square region, and its stability is determined by $F'(\theta^*)$ for a unique fixed point $\theta^* = \pi/2 - F(\theta^*)$ [5]. Note that closed square orbits also naturally appear in nonlinear dissipative physical systems with spatially localized structures in square stadia or cavities, quite different from floating camphor disks (see, for example, [23] and [12]).

A particle model in the half-plane $\{(x, y) \in \mathbb{R}^2 \mid x > 0\}$ is studied:

$$\begin{cases} \dfrac{dx}{dt} = v + m_0 h_a(x), \\ \dfrac{dy}{dt} = w, \\ \dfrac{dv}{dt} = v\left[\delta - m_1(v^2 + w^2)\right] + m_2 h_a(x), \\ \dfrac{dw}{dt} = w\left[\delta - m_1(v^2 + w^2)\right], \end{cases} \tag{1}$$

where (x, y) is the position of the particle, m_0, m_1, m_2, a and δ are parameters, and h_a is the function given by

$$h_a(r) = \frac{e^{-2ar}}{\sqrt{2r}}. \tag{2}$$

In addition, (v, w) represents the deformation in profile of a traveling spot from a stationary spot. It is closely related to the velocity.

In this study, the following assumptions are imposed:

$$m_0 \geq 0, \quad m_1 > 0, \quad m_2 > 0, \quad a > 0, \tag{3}$$

$$\delta > 0 \quad \text{and} \quad m_0\delta < m_2. \tag{4}$$

Note that m_0, m_1, m_2 and a are determined by a spot solution of a reaction-diffusion system [3, 6]. It is known that these parameters, except m_1, satisfy (3) above for the moving boundary model of camphor disk motion [3]. Although the sign of m_1 is not known, numerical simulations suggest it is positive for our model. We assume $\delta > 0$ in order to be sure that the particle does move. If $m_0\delta \geq m_2$ holds, then equilibria of (1) exist. Since the particle model was derived under the assumption of small δ, and the appearance of equilibria represents a qualitative change in model dynamics, we will henceforth assume (4). We note in passing that rich behavioral diversity is also predicted to be exhibited by self-propelling microscopic particles having surfaces composed of

regions with distinct physical properties (Janus particles) moving in solution near a boundary [29].

The $h_a(x)$ terms represent repulsive interaction between the particle and the boundary. One can show that if $x(0) > 0$ and $v(0) < 0$, then there exists a unique $t_0 > 0$ such that $v(t_0) = 0$ and $v(t) > 0$ for any $t > t_0$. In other words, the particle reflects. See [5] for details. Far from the boundary, the speed of the particle converges to $\sqrt{\delta/m_1}$. As is standard in scattering theory, we study only reflections for which the particle comes "from infinity" and returns "to infinity". In both cases, the speed "at infinity" is $\sqrt{\delta/m_1}$.

To be more precise, let $z = h_a(x)$ and consider equations for (z, v, w):

$$\begin{cases} \dfrac{dz}{dt} = H(z)(v + m_0 z), \\ \dfrac{dv}{dt} = v\left[\delta - m_1(v^2 + w^2)\right] + m_2 z, \\ \dfrac{dw}{dt} = w\left[\delta - m_1(v^2 + w^2)\right], \end{cases} \tag{5}$$

where $H(z) = h_a'(h_a^{-1}(z))$. It is known that, for any $\theta_{\rm inc} \in [0, \pi/2]$, there exists a $\theta_{\rm ref} \in [0, \pi/2]$ and a solution $(z(t), v(t), w(t))$ such that

$$\lim_{t\to\pm\infty} z(t) = 0, \quad \lim_{t\to\pm\infty} \left((v(t))^2 + (w(t))^2\right) = \frac{\delta}{m_1} \tag{6}$$

and

$$\lim_{t\to-\infty} \tan^{-1}\left(\frac{w(t)}{-v(t)}\right) = \theta_{\rm inc}, \quad \lim_{t\to\infty} \tan^{-1}\left(\frac{w(t)}{v(t)}\right) = \theta_{\rm ref} \tag{7}$$

(see [5]). $\theta_{\rm inc}$ and $\theta_{\rm ref}$ are the angles of incidence and reflection, respectively. Therefore, $\theta_{\rm ref}$ is a function of $\theta_{\rm inc} \in [0, \pi/2]$. The functional relation $\theta_{\rm ref} = F(\theta_{\rm inc})$ in the low speed limit is studied here. Note that F is parametrized by δ, m_0, m_1, m_2 and a. There is one special case of reflection, for which the particle moves only perpendicular to the boundary but infinitely far from it. In that case, $\dot{y}(t) = w(t)$ is always zero, $y(t)$ is constant, and $\theta_{\rm ref} = \theta_{\rm inc} = 0$. On the other hand, $(z(t), v(t), w(t)) = (0, 0, \sqrt{\delta/m_1})$ is a stationary solution, which corresponds to a straight-line orbit parallel to the y-axis at infinity. For this case, $\theta_{\rm ref} = \theta_{\rm inc} = \pi/2$. F is continuous on $[0, \pi/2]$ because it is defined by a continuous family of heteroclinic solutions of (5).

As $w(0) = 0$ implies $w(t) \equiv 0$ and the system (1) commutes with $(y, w) \mapsto (-y, -w)$, we may assume $w(t) > 0$ for all t without loss of generality. [5] have proved the inequality $\theta_{\rm ref} \geq \theta_{\rm inc}$ under the assumption that m_0 is equal to zero. Their proof is based on a phase-space analysis of nonlinear ordinary differential equations for (z, v, w). We believe that this assumption can be removed and that the inequality holds for any parameter set satisfying (3) and (4).

Note that we are not intending to study only a specific system. Indeed, (1) represents a universal property of spot dynamics in planar reaction-diffusion systems (planar RDS) because (1) with $m_0 = m_2 = 0$ describes motions of the spot on the entire plane, and it is nothing but a normal form of a pitchfork

bifurcation of revolution. The function h_a is derived from the asymptotic profile of stationary spots for planar RDS. If motion of a self-propelling particle arises due to a pitchfork bifurcation, then it will be described by (1) but possibly with different interaction terms (i.e. h_a), although the low speed limit we consider makes use only of the asymptotic behavior of h_a when the particle is very far from the boundary, and this asymptotic behavior is fixed in the planar RDS for camphor disks our particle model is derived from [3], and also in the more general planar RDS [6]. Traveling spots in general reaction-diffusion systems can exhibit much richer dynamics [19, 27, 20]. Our intention is to reveal a universal property of a spot that slowly moves and repulsively interacts with the boundary in particular.

In this paper, we propose the following Main Conjecture, which represents the first quantitative reflection rule for a particle model of this kind:

Main Conjecture. *As* $\delta \to 0$*,*

$$\theta_{\text{ref}} \approx \theta_{\text{inc}} + \frac{4}{3}\left(1 + \frac{m_0 a^2}{m_1 m_2}\right)\frac{\sqrt{\delta m_1}}{a}\sin\theta_{\text{inc}}\cos^2\theta_{\text{inc}}. \tag{8}$$

More precisely, for any m_0*,* m_1*,* m_2 *and* a *satisfying* (3)*, and* $\theta_{\text{inc}} \in (0, \pi/2)$*,*

$$\lim_{\delta\to 0} F(\theta_{\text{inc}}) = \theta_{\text{inc}} \tag{9}$$

and

$$\lim_{\delta\to 0} \frac{F(\theta_{\text{inc}}) - \theta_{\text{inc}}}{\frac{\sqrt{\delta m_1}}{a}\sin\theta_{\text{inc}}\cos^2\theta_{\text{inc}}} = \frac{4}{3}\left(1 + \frac{m_0 a^2}{m_1 m_2}\right). \tag{10}$$

The present paper is organized as follows. In the next section, we derive a very rough approximation which provided the angular dependency of the series of conjectures put forward in Section 3. Section 4 is devoted to numerical experiments which support, and in some cases suggested, the conjectures.

First, it will be useful to illustrate our Main Conjecture with a generic example, and use this to provide an overview of what is to come.

1.1 A Generic Example

The parameter set

$$m_0 = \frac{17}{23}, \quad m_1 = \frac{5}{6}, \quad m_2 = \frac{7}{19}, \quad a = \frac{11}{10} \quad \text{and} \quad \theta_{\text{inc}} = \frac{28}{33}\,\text{rad} \tag{11}$$

will serve to define our generic example.

We have

$$\theta_{\text{inc}} \approx 0.84848484848484848485\,, \tag{12}$$

and can calculate θ_{ref} for $\delta = 10^{-2}$, using any of the numerical methods described in Section 4, getting the result

$$\theta_{\text{ref}} \approx 0.98346783839309184712\,. \tag{13}$$

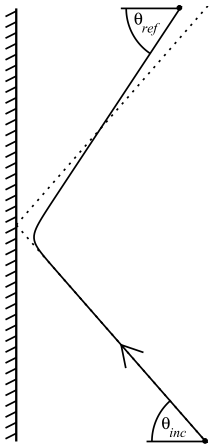

Figure 1: Quantitatively accurate geometry of nonspecular reflection for the generic example with with parameters $m_0 = 17/23$, $m_1 = 5/6$, $m_2 = 7/19$, $a = 11/10$, $\theta_{\rm inc} = 28/33$, and $\delta = 10^{-2}$. The continuous curve represents the trajectory of a particle reflecting off a boundary wall, coming "from infinity" at the bottom right and returning "to infinity" at the top right. The fact that the reflection is nonspecular ($\theta_{\rm ref} \neq \theta_{\rm inc}$) is shown using the comparison with a standard mathematical billiard particle following the dotted line trajectory, which actually hits the wall, and for which the angles of incidence and reflection must be equal. The x axis is horizontal, with $x = 0$ at the face of the boundary wall. The y axis is vertical.

Note that $\theta_{\rm ref}$ is larger than $\theta_{\rm inc}$, as expected. This nonspecular reflection is illustrated in Figure 1.

A very rough approximation of the process of reflection, described in Section 2, led to the suggestion that, in a low speed limit (i.e. small δ), the difference between $\theta_{\rm inc}$ and $\theta_{\rm ref}$ should depend upon δ and $\theta_{\rm inc}$ according to

$$\theta_{\rm ref} - \theta_{\rm inc} \propto \sqrt{\delta} \sin\theta_{\rm inc} \cos^2\theta_{\rm inc} \qquad \text{(approximate, for small } \delta\text{)}. \tag{14}$$

It is useful to express this in terms of (cf. equation (47) of Conjecture 1)

$$\underline{K}(\delta, m_0, m_1, m_2, a, \theta_{\rm inc}) = \frac{\theta_{\rm ref} - \theta_{\rm inc}}{\sqrt{\delta} \sin\theta_{\rm inc} \cos^2\theta_{\rm inc}}. \tag{15}$$

Table 1 provides the kind of numerical values which suggested that (i) the angle of reflection equals the angle of incidence in the limit that δ goes to zero and (ii) the limit of $\underline{K}(\delta, m_0, m_1, m_2, a, \theta_{\rm inc})$ as δ goes to zero appears to exist. What is expressed in Conjecture 1, which was based upon many more numerical experiments with other parameter sets, is stronger, since it asserts that the limit of $\underline{K}$ as δ goes to zero does not depend upon $\theta_{\rm inc}$:

$$\lim_{\delta\to 0} \underline{K}(\delta, m_0, m_1, m_2, a, \theta_{\rm inc}) = K(m_0, m_1, m_2, a). \tag{16}$$

Table 1: Angles of reflection for the generic example with parameters $m_0 = 17/23$, $m_1 = 5/6$, $m_2 = 7/19$, $a = 11/10$ and $\theta_{\text{inc}} = 28/33$ rad, calculated for decreasing values of δ. The second and third columns directly relate to equations (46) and (47) of Conjecture 1, respectively.

δ	$\theta_{\text{ref}} = F(\theta_{\text{inc}})$	$\underline{K}(\delta, m_0, m_1, m_2, a, \theta_{\text{inc}})$
10^{-10}	0.84850214756489326921	6.35655335594364
10^{-20}	0.84848484865687756183	6.32121479167490
10^{-30}	0.84848484848485020198	6.30960717019543
10^{-40}	0.84848484848484848487	6.30385245964328
10^{-50}	0.84848484848484848485	6.30041810036372

That reflection should be specular in the limit that δ goes to zero is consistent with the Hamiltonian limit (see Section 2.2), for which reflection is necessarily specular, of the model (1) as δ goes to zero.

The limit of $\underline{K}$ was difficult to pin down numerically because convergence is slow, and conjectures 1 to 3 involve successive reductions of the number of functions of parameters required to specify it, in the hope that that would lead to greater clarity. This progression can perhaps best be described in terms of the identities (this is equation (51))

$$K(m_0, m_1, m_2, a) = \frac{\sqrt{m_1}}{a} K\left(\frac{m_0 m_1}{\sqrt{a}}, 1, \frac{m_1^2 m_2}{a^{\frac{5}{2}}}, 1\right) \tag{17}$$

and (combining equations (55) and (56))

$$K(\alpha, 1, \beta, 1) = \kappa(\alpha, \beta) = \chi\left(\frac{\alpha}{\beta}\right), \tag{18}$$

which arose from the use of symmetry arguments (see Section 3) and numerical experimentation (Section 4.3).

The conjectured limit for $\delta \to 0$ is (see equations (53), (57) and (10))

$$\kappa\left(\frac{m_0 m_1}{\sqrt{a}}, \frac{m_1^2 m_2}{a^{\frac{5}{2}}}\right) = \chi\left(\frac{m_0 a^2}{m_1 m_2}\right) = \frac{4}{3}\left(1 + \frac{m_0 a^2}{m_1 m_2}\right). \tag{19}$$

For the specific parameter choices of this generic example, the value is $314998/60375 \approx 5.217358178053830$.

In Figure 2 and Table 2, we can see the slow convergence directly. Towards the end of Section 4.3, high precision numerical experiments are described, in which empirical values of κ, denoted by $\underline{\kappa}$ (see equation (67)), were studied. To be more specific, values of $\underline{\kappa}(\delta, r, 1, 1, 1, \theta_{\text{inc}})$ were calculated for various values of r (this stands in for m_0/m_2) and very small δ, leading to the conclusion that the next leading term in the asymptotic expansion of κ behaves either as $1/\ln\delta$ (the generic case) or $1/\ln^2\delta$ (for $m_0/m_2 = 1$ only). This suggests the idea that

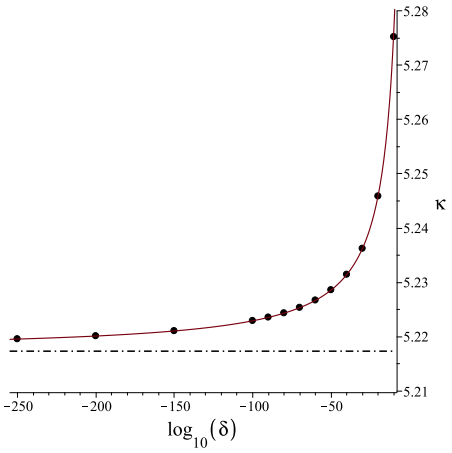

Figure 2: Values of $\underline{\kappa}(\delta, m_0, m_1, m_2, a, \theta_{\text{inc}})$ for the generic example with with parameters $m_0 = 17/23$, $m_1 = 5/6$, $m_2 = 7/19$, $a = 11/10$ and $\theta_{\text{inc}} = 28/33$ rad, calculated for decreasing values of δ (moving left). The dashed horizontal line indicates the conjectured limiting value of $\underline{\kappa}$ (i.e. κ itself).

the next leading term after κ is $O(1/|\ln\delta|)$ (compare with equation (69), which applies to θ_{ref} directly).

Since we are discussing a specific generic example for which m_0/m_2 is not equal to one, we can demonstrate the accuracy of the conjectured limit by adding a correction to $\underline{\kappa}$ which should bring it closer to that limit. Since it appears that the next leading terms may behave as $1/\ln\delta$ and $1/\ln^2\delta$, we expect that it should be possible to construct a linear combination of these which can be added to the slowly converging $\underline{\kappa}$ values so that convergence appears to be greatly sped up. Indeed, the function

$$f(\delta) = \frac{0.555}{|\log_{10}(\delta)|} + \frac{0.384}{|\log_{10}(\delta)|^2} \tag{20}$$

is sufficient for this purpose. The third column of Table 2, which is the result of adding this correction, clearly does converge much faster to the conjectured limit.

This ends our discussion of the one generic example. The intention has been to prepare the reader for what is to come.

Table 2: Values of $\underline{\kappa}(\delta, m_0, m_1, m_2, a, \theta_{\text{inc}})$ for the generic example with parameters $m_0 = 17/23$, $m_1 = 5/6$, $m_2 = 7/19$, $a = 11/10$ and $\theta_{\text{inc}} = 28/33$ rad, calculated for decreasing values of δ. The values in the third column are the sum of the corresponding $\underline{\kappa}$ values in the second column with the correction $f(\delta)$, defined in equation (20), which acts to speed up convergence. The bottom row shows the conjectured limit as δ goes to zero.

δ	$\underline{\kappa}\left(\delta, \frac{17}{23}, \frac{5}{6}, \frac{7}{19}, \frac{11}{10}, \frac{28}{33}\right)$	$\underline{\kappa}(\delta, \dots) + f(\delta)$
10^{-20}	5.245866563993426	5.21727
10^{-30}	5.236233600170267	5.21735
10^{-40}	5.231457865653101	5.21736
10^{-50}	5.228607750428873	5.21736
10^{-60}	5.226714780343825	5.21736
10^{-70}	5.225366425705772	5.21736
10^{-80}	5.224357351520029	5.21736
10^{-90}	5.223573882470851	5.21736
10^{-100}	5.222948005645642	5.21736
10^{-150}	5.221075495033316	5.21736
10^{-200}	5.220142361168298	5.21736
10^{-250}	5.219583577821452	5.21736
$\delta \to 0$	5.217358178053830	5.21736

2 Rough approximation

2.1 First exploration

To begin with, let us define

$$v_{\text{inc}} = -\sqrt{\frac{\delta}{m_1}}\cos\theta_{\text{inc}}, \quad w_{\text{inc}} = \sqrt{\frac{\delta}{m_1}}\sin\theta_{\text{inc}}, \tag{21}$$

$$v_{\text{ref}} = \sqrt{\frac{\delta}{m_1}}\cos\theta_{\text{ref}}, \quad w_{\text{ref}} = \sqrt{\frac{\delta}{m_1}}\sin\theta_{\text{ref}}. \tag{22}$$

If one plots $w(t)$ against $v(t)$ (as in Figure 3), it seems that for the most part $w(t)$ can be approximated as a linear function of $v(t)$, and that as δ becomes smaller the slope decreases to the point where one might reasonably write $v_{\text{ref}} \approx -v_{\text{inc}}$ and $w_{\text{ref}} \approx w_{\text{inc}}$. Although it is not guaranteed that $w(t)$ can indeed be expressed as a function of $v(t)$ nor that $v'(t) \neq 0$ in general, one can formally construct

$$\frac{d\tilde{w}}{d\tilde{v}}(\tilde{v}) = \frac{\tilde{w}(\tilde{v})\left[\delta - m_1(\tilde{v}^2 + (\tilde{w}(\tilde{v}))^2)\right]}{\tilde{v}\left[\delta - m_1(\tilde{v}^2 + (\tilde{w}(\tilde{v}))^2)\right] + m_2 h_a(\tilde{x}(\tilde{v}))}, \tag{23}$$

where $\tilde{x}(\tilde{v}) = x(v^{-1}(\tilde{v})), \tilde{w}(\tilde{v}) = w(v^{-1}(\tilde{v}))$, and $v^{-1}(\tilde{v})$ is the inverse function

of $t \mapsto v(t) = \tilde{v}$. Expanding around $\tilde{v} = 0$, we have

$$\tilde{w}(\tilde{v}) = w(0) + \frac{\tilde{w}(0)(\delta - m_1(\tilde{w}(0))^2)}{m_2 h_a(\tilde{x}(0))}\tilde{v} + O(\tilde{v}^2). \tag{24}$$

w_{ref} and w_{inc} are given by

$$w_{\text{ref}} \approx w(0) + \frac{\tilde{w}(0)(\delta - m_1(\tilde{w}(0))^2)}{m_2 h_a(\tilde{x}(0))}v_{\text{ref}}, \tag{25}$$

$$w_{\text{inc}} \approx w(0) + \frac{\tilde{w}(0)(\delta - m_1(\tilde{w}(0))^2)}{m_2 h_a(\tilde{x}(0))}v_{\text{inc}}. \tag{26}$$

As we are assuming $v_{\text{ref}} - v_{\text{inc}} \approx 2|v_{\text{inc}}|$, we have

$$w_{\text{ref}} \approx w_{\text{inc}} + \frac{\tilde{w}(0)(\delta - m_1(\tilde{w}(0))^2)}{m_2 h_a(\tilde{x}(0))} \times (2|v_{\text{inc}}|). \tag{27}$$

By (26), $\tilde{w}(0) \approx w_{\text{inc}} + O(v_{\text{inc}})$. As we have $m_1(v_{\text{inc}}^2 + w_{\text{inc}}^2) = \delta$, we obtain rough approximations:

$$v_{\text{ref}} \approx -v_{\text{inc}}, \tag{28}$$

$$w_{\text{ref}} \approx w_{\text{inc}} + \frac{m_1 w_{\text{inc}} v_{\text{inc}}^2}{m_2 h_a(\tilde{x}(0))} \times (2|v_{\text{inc}}|), \tag{29}$$

and therefore

$$\theta_{\text{ref}} \approx \tan^{-1}\left(-\frac{w_{\text{inc}}}{v_{\text{inc}}} + 2\frac{m_1 w_{\text{inc}} v_{\text{inc}}^2}{m_2 h_a(\tilde{x}(0))}\right). \tag{30}$$

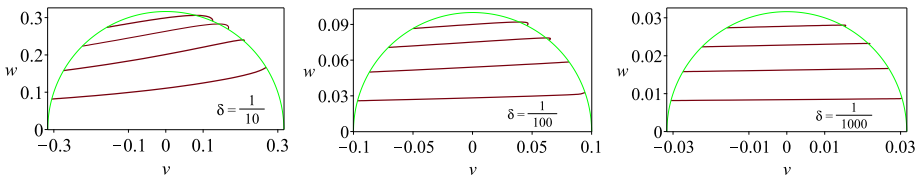

Figure 3: Plots of $w(t)$ against $v(t)$ for trajectories defined by angles of incidence $\theta_{\text{inc}} \in \{\pi/12, \pi/6, \pi/4, \pi/3\}$. The green semicircles represent the condition $v_{\text{inc}}^2 + w_{\text{inc}}^2 = v_{\text{ref}}^2 + w_{\text{ref}}^2$ "at infinity". As δ becomes smaller, from left to right, trajectories appear to become straighter and more horizontal.

We can evaluate the right hand side if we have an estimate for $\tilde{x}(0)$, which is the value of $x(t_0)$ at the time t_0 when $v(t_0) = 0$. Alternatively, it would suffice if a direct approximation of $h_a(\tilde{x}(0)) = h_a(x(t_0))$ were available. We consider a "low speed" limit to obtain the approximation.

2.2 Hamiltonian Limit

Since we are assuming $m_0\delta < m_2$, we can define a scaled time τ

$$dt = \frac{d\tau}{1 - \dfrac{m_0}{m_2}\delta + \dfrac{m_0 m_1}{m_2}(v^2(t) + w^2(t))}, \tag{31}$$

and coordinates

$$(x_s(\tau), y_s(\tau), v_s(\tau), w_s(\tau)) = \left(x(t) - \frac{m_0}{m_2}v(t), y(t) - \frac{m_0}{m_2}w(t), v(t), w(t)\right), \tag{32}$$

for which one can transform (1) into the form

$$\begin{cases} \dfrac{dx_s}{d\tau}(\tau) = v_s(\tau), \\ \dfrac{dy_s}{d\tau}(\tau) = w_s(\tau), \\ \dfrac{dv_s}{d\tau}(\tau) = F_x(x_s(\tau), v_s(\tau), w_s(\tau)), \\ \dfrac{dw_s}{d\tau}(\tau) = F_y(v_s(\tau), w_s(\tau)) \end{cases} \tag{33}$$

with

$$F_x(x, v, w) = \frac{v\left(\delta - m_1(v^2 + w^2)\right) + m_2 h_a(x + \frac{m_0}{m_2}v)}{1 - \frac{m_0}{m_2}\delta + \frac{m_0 m_1}{m_2}(v^2 + w^2)} \tag{34}$$

and

$$F_y(v, w) = \frac{w\left(\delta - m_1(v^2 + w^2)\right)}{1 - \frac{m_0}{m_2}\delta + \frac{m_0 m_1}{m_2}(v^2 + w^2)}. \tag{35}$$

There are various possible ways of defining the low speed limit of F_x and F_y. For the purpose of obtaining the simplest nontrivial approximation for $h_a(\hat{x}(0))$, one can simply set $\delta = v_s(\tau) = w_s(\tau) = 0$ to get the zeroth-order terms

$$F_x^{(0)}(x_s(\tau), v_s(\tau), w_s(\tau)) = m_2 h_a(x_s(\tau)), \tag{36}$$

$$F_y^{(0)}(v_s(\tau), w_s(\tau)) = 0, \tag{37}$$

and the corresponding system

$$\begin{cases} \dfrac{d^2x_s}{d\tau^2}(\tau) = m_2 h_a(x_s(\tau)), \\ \dfrac{d^2y_s}{d\tau^2}(\tau) = 0, \end{cases} \tag{38}$$

which is an integrable Hamiltonian system with kinetic energy

$$T(v, w) = \frac{1}{2}(v^2 + w^2) \tag{39}$$

and potential energy

$$V(x) = \frac{m_2}{2}\sqrt{\frac{\pi}{a}}\left(1 - \mathrm{erf}(\sqrt{2ax})\right). \tag{40}$$

Solution curves of (38) are as shown in Figure 4. In the low speed limit, the closest approach to the boundary will be far from it. Correspondingly, by the asymptotic expansion of the error function, we find

$$V(x) \sim \frac{\sqrt{2}m_2 \exp(-2ax)}{4a\sqrt{x}} = \frac{m_2 h_a(x)}{2a} \quad (x \to \infty). \tag{41}$$

As we consider the trajectory of a particle whose speed is $\sqrt{\delta/m_1}$ at $x \to \infty$, the potential energy is zero and the kinetic energy is equal to $\delta/(2m_1)$ when the particle is infinitely far from the boundary. At the point of closest approach to the boundary, $v_s = 0$ but w_s is unchanged and has the value $\sqrt{\delta/m_1}\sin\theta_{\mathrm{inc}}$. Conservation of energy implies

$$\frac{m_2 h_a(x_s)}{2a} = \frac{\delta}{2m_1}\cos^2\theta_{\mathrm{inc}}, \tag{42}$$

providing us with the desired approximation of $h_a(\hat{x}(0))$. Therefore, the simple approximation we have been searching for is

$$h_a(\hat{x}(0)) = \frac{a\delta\cos^2\theta_{\mathrm{inc}}}{m_1 m_2}. \tag{43}$$

Inserting (43) into (30), we obtain

$$\theta_{\mathrm{ref}} \approx \tan^{-1}\left(\tan\theta_{\mathrm{inc}} + \frac{2m_1 w_{\mathrm{inc}} v_{\mathrm{inc}}^2}{a\delta\cos^2\theta_{\mathrm{inc}}}\right). \tag{44}$$

Since we are considering only the limit of small δ, this can be further approximated by

$$\theta_{\mathrm{ref}} \approx \theta_{\mathrm{inc}} + \frac{2\sqrt{\delta m_1}}{a}\sin\theta_{\mathrm{inc}}\cos^2\theta_{\mathrm{inc}}, \tag{45}$$

and this is a complete approximation of the angle of reflection as a function of the angle of incidence, based upon the very rough approximation we have described. Is it accurate? As Figure 5 shows, it seems to have something close to the right shape, but otherwise fails as an approximation. However, there was a hint (see Figure 6) that perhaps the error could be repaired by the introduction of a scaling factor. This line of thought led directly to Conjecture 1, stated in the following section.

3 Conjectures

Conjecture 1. *For any m_0, m_1, m_2 and a satisfying* (3)*, there exists a positive constant K such that for any $\theta_{\mathrm{inc}} \in (0, \pi/2)$,*

$$\lim_{\delta\to 0} F(\theta_{\mathrm{inc}}) = \theta_{\mathrm{inc}} \tag{46}$$

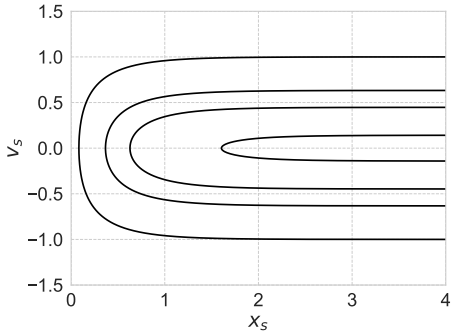

Figure 4: Trajectories of (x_s, v_s) of the integrable Hamiltonian system (38).

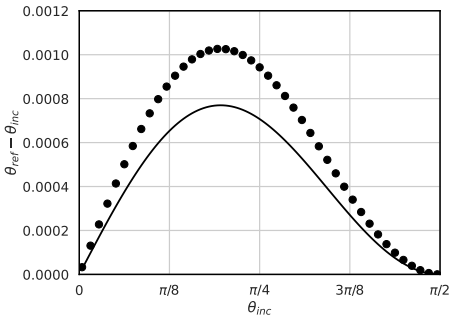

Figure 5: Numerically computed angle relation (dots) for $\delta = 10^{-6}, m_0 = m_1 = m_2 = a = 1$, and the rough approximation (45) (solid). The vertical axis indicates $\theta_{\rm ref} - \theta_{\rm inc}$.

and

$$\lim_{\delta\to 0} \frac{F(\theta_{\rm inc}; \delta, m_0, m_1, m_2, a) - \theta_{\rm inc}}{\sqrt{\delta}\sin\theta_{\rm inc}\cos^2\theta_{\rm inc}} = K(m_0, m_1, m_2, a). \tag{47}$$

K, being function of four variables, would appear to be difficult to investigate, but it is not entirely without structure. If $x_1(t)$, $y_1(t)$, $v_1(t)$ and $w_1(t)$ satisfy (1) with parameters $\delta = \hat{\delta}$, $m_0 = \hat{m}_0$, $m_1 = \hat{m}_1$, $m_2 = \hat{m}_2$ and $a = \hat{a}$, then $(x_2(t), y_2(t), v_2(t), w_2(t)) = (x_1(st), y_1(st), sv_1(st), sw_1(st))$ satisfies the same system for any positive s, but with parameters $\delta = s\hat{\delta}$, $m_0 = s\hat{m}_0$, $m_1 = \hat{m}_1/s$, $m_2 = s^2\hat{m}_2$ and $a = \hat{a}$. Since the trajectories traced out by $(x_1(t), y_1(t))$ and $(x_2(t), y_2(t))$ are identical, angles of incidence and reflection will also be identical. It follows that

$$K(sm_0, s^{-1}m_1, s^2m_2, a) = \frac{1}{\sqrt{s}}K(m_0, m_1, m_2, a) \tag{48}$$

for any $s > 0$.

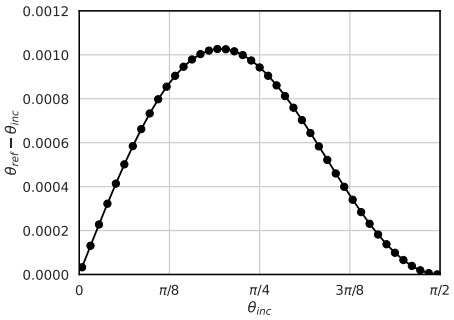

Figure 6: Numerically computed angle relation (dots) for $\delta = 10^{-6}, m_0 = m_1 = m_2 = a = 1$ and $(8/3)\sqrt{\delta}\sin\theta_{\rm inc}\cos^2\theta_{\rm inc}$ (solid), which differs from the rough approximation (45) illustrated in Figure 5 only by a constant rational scaling factor. The vertical axis indicates $\theta_{\rm ref} - \theta_{\rm inc}$.

Furthermore, a consequence of (2) is that $(x_3(t), y_3(t), v_3(t), w_3(t)) = (sx_1(t), sy_1(t), sv_1(t), sw_1(t))$ also satisfies the same system, but with parameters $\delta = \hat{\delta}$, $m_0 = s^{3/2}\hat{m}_0$, $m_1 = \hat{m}_1/s^2$, $m_2 = s^{3/2}\hat{m}_2$ and $a = \hat{a}/s$. The trajectories traced out by $(sx_1(t), sy_1(t))$ and $(x_3(t), y_3(t))$ are identical, so angles of incidence and reflection will also be identical, providing a second identity:

$$K(s^{3/2}m_0, s^{-2}m_1, s^{3/2}m_2, s^{-1}a) = K(m_0, m_1, m_2, a) \tag{49}$$

for any $s > 0$.

Combining these two identities, we are able to reduce K to a form which depends upon only two parameters:

$$\begin{aligned} K(m_0, m_1, m_2, a) &= K\left(a^{\frac{3}{2}}m_0, \frac{m_1}{a^2}, a^{\frac{3}{2}}m_2, 1\right) &(50)\\ &= \frac{\sqrt{m_1}}{a}K\left(\frac{m_0 m_1}{\sqrt{a}}, 1, \frac{m_1^2 m_2}{a^{\frac{5}{2}}}, 1\right) &(51)\\ &= \frac{\sqrt{m_1}}{a}\kappa\left(\frac{m_0 m_1}{\sqrt{a}}, \frac{m_1^2 m_2}{a^{\frac{5}{2}}}\right). &(52)\end{aligned}$$

It is likely significant that the factor $\sqrt{m_1}/a$ also appeared in (45). This leads to a refined conjecture:

Conjecture 2. *There is a positive function $\kappa : \mathbb{R}^2 \to \mathbb{R}$ such that for any m_0, m_1, m_2 and a satisfying* (3)*, and $\theta_{\rm inc} \in (0, \pi/2)$,*

$$\lim_{\delta\to 0} \frac{F(\theta_{\rm inc}; \delta, m_0, m_1, m_2, a) - \theta_{\rm inc}}{\frac{\sqrt{\delta m_1}}{a}\sin\theta_{\rm inc}\cos^2\theta_{\rm inc}} = \kappa\left(\frac{m_0 m_1}{\sqrt{a}}, \frac{m_1^2 m_2}{a^{\frac{5}{2}}}\right). \tag{53}$$

One can also use the two symmetries described above to reduce the dimension of the parameter space, facilitating numerical experimentation:

$$F(\theta_{\rm inc}; \delta, m_0, m_1, m_2, a) = F\left(\theta_{\rm inc}; \frac{m_1}{a^2}\delta, \frac{m_0 m_1}{\sqrt{a}}, 1, \frac{m_1^2 m_2}{a^{\frac{5}{2}}}, 1\right). \tag{54}$$

Since $(m_1/a^2)\delta$ satisfies (4) if δ satisfies (4) and m_1 satisfies (3), and both $m_0 m_1/\sqrt{a}$ and $m_1^2 m_2/a^{5/2}$ satisfy (3) if m_0, m_1, m_2 and a satisfy (3), it is only absolutely necessary to perform numerical experiments using reduced parameter sets for which $m_1 = a = 1$, although we have also allowed m_1 and a to be free (while still satisfying (3)) from time to time as a sanity check.

By the above symmetry arguments, Conjecture 1 implies Conjecture 2. Further progress was dependent upon numerical experiments, details of which will be presented in the next section.

Note that

$$\kappa(\alpha, \beta) = K(\alpha, 1, \beta, 1) \tag{55}$$

could be expected to have values roughly near 2, in accordance with (45), but large deviations are in fact observed. Moreover, in a detailed numerical study of the values of $\kappa(\alpha, \beta)$ (see Figures 7 and 8), it was observed that the values of κ seem to depend only upon the ratio α/β. This suggested the existence of a further identity:

$$\kappa(\alpha, \beta) = \chi\left(\frac{\alpha}{\beta}\right). \tag{56}$$

Conjecture 3. *There is a positive function $\chi : \mathbb{R} \to \mathbb{R}$ such that for any m_0, m_1, m_2 and a satisfying* (3)*, and $\theta_{\rm inc} \in (0, \pi/2)$,*

$$\lim_{\delta \to 0} \frac{F(\theta_{\rm inc}; \delta, m_0, m_1, m_2, a) - \theta_{\rm inc}}{\frac{\sqrt{\delta m_1}}{a} \sin\theta_{\rm inc} \cos^2\theta_{\rm inc}} = \chi\left(\frac{m_0 a^2}{m_1 m_2}\right). \tag{57}$$

Note that F is not determined only by $m_0 a^2/(m_1 m_2)$ if $\delta > 0$. Nevertheless, it is expected that the univariate function χ appears in the limit $\delta \to 0$. This is illustrated in Figure 7.

Further numerical experiments (described in the following section) for extremely small values of δ suggested that the function $\chi(r)$ may have the simple form

$$\chi(r) = \frac{4}{3}(1 + r), \tag{58}$$

which brings us to our Main Conjecture.

4 Numerical Experiments

A representative selection of the numerical experiments we conducted, which all supported the conjectures above, is presented in this section. Calculations were performed on a variety of computers, including the MIMS Shared Memory Processor (MIMS SMP) of the Meiji University Center for Mathematical Modeling and Applications (CMMA), which was used for many of the longest runs (exceeding one month CPU time).

The particle model (1), or a slightly modified version of it, can be numerically integrated using standard interactive software tools using multiple-precision floating-point arithmetic, such as Maple [15], for values of δ larger

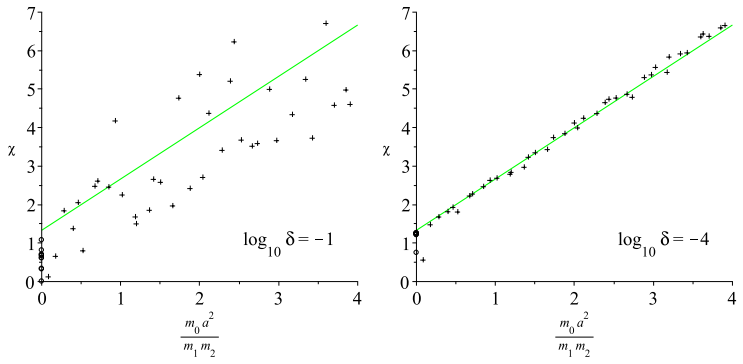

Figure 7: As δ becomes smaller, from the left-hand to the right-hand plot, the empirical values of χ approach a linear function (the green line) of $m_0a^2/(m_1m_2)$. It is in this sense that we state that the univariate function $\chi(r) = (4/3)(1 + m_0a^2/(m_1m_2))$ (equation (58)) appears in the limit of $\delta \to 0$. The points in these plots correspond to a fixed set of parameter sets, for which m_0, m_1, m_2 and a have been chosen randomly from $(0, 4]$ and $\theta_{\rm inc}$ from $[0.1, 1.5]$, and a total of 40 sets (crosses) chosen such that their horizontal distribution in the plot appears to be even. An additional ten points (circles) were generated in the same way, but with m_0 set to zero. Only the values of δ differ between the two plots.

than about 10^{-30}, but we wanted to reach much smaller values to increase our confidence in the conjectures above, and found it useful to develop our own codes to gain more control over adaptive step-size decisions and memory management. Detailed comparisons were performed in cases where more than one method provided an estimate of a result, allowing us to be confident that our codes were functioning as intended.

For very small values of δ, we used two methods of numerical integration:

- An explicit Runge-Kutta method of order 9 (see Table 8 of [30]), implemented using the MPFR library [7].
- The Taylor expansion method implemented in the CAPD library [31], which we compiled with the MPFR library [7]. We used multiple-precision floating-point arithmetic rather than interval arithmetic.

The second method was able to deal with the smallest values of δ (down to 10^{-250}) we investigated.

Instead of dealing with (1) directly, we solved modified systems. Remark that we do not have to solve the equation for y because y, which is just an integral of w, is irrelevant to the definition of angles.

4.1 Explicit Runge-Kutta Method of order 9

The point of view taken for this method was to focus on the ratio v/w, since that is directly related to the angles we are interested in and increases monotonically with time, and also to choose and/or scale coordinates with the intention of avoiding extremely large numbers.

Let

$$z(t) = \frac{1}{x(t)}, \quad r(t) = \frac{v(t)}{w(t)}, \quad s(t) = \sqrt{\frac{m_1}{\delta}}\, w(t) \tag{59}$$

and

$$b(t) = \sqrt{\frac{m_1}{\delta}}\, h_a\left(\frac{1}{z(t)}\right). \tag{60}$$

Note that we can assume that $s(t) > 0$.

To study the relationship between angles of incidence and reflection, the equations that need to be integrated are

$$\frac{d\,z(t)}{dt} = -\sqrt{\frac{\delta}{m_1}}\left(\, r(t)\, s(t) + m_0\, b(t)\,\right) z^2(t) \tag{61}$$

$$\frac{d\,r(t)}{dt} = \frac{m_2\, b(t)}{s(t)} \tag{62}$$

$$\frac{d\,s(t)}{dt} = \delta\, s(t)\left(\, 1 - s^2(t)\left(\, 1 + r(t)^2\,\right)\right), \tag{63}$$

with initial conditions (for some suitably large $X > 0$)

$$z(0) = \frac{1}{X}, \quad r(0) = -\cot\theta_{\rm inc}, \quad s(0) = \sin\theta_{\rm inc}. \tag{64}$$

The angle of reflection is given by

$$\theta_{\rm ref} = \lim_{t\to\infty} \tan^{-1}\frac{1}{r(t)}. \tag{65}$$

Integration continues until at least $r(t) > 0$ and $z(t) < 1/X$.

4.2 Taylor Expansion Method

Let $z = 1/x$. Multiplying $\sqrt{2x}/\sqrt{\delta}$ by the right hand side of (1), we obtain

$$\begin{cases} \dfrac{dz}{dt} = -\dfrac{z^2}{\sqrt{\delta}}\left(\sqrt{\dfrac{2}{z}}v + m_0 e^{-2az^{-1}}\right), \\ \dfrac{dv}{dt} = \dfrac{1}{\sqrt{\delta}}\left(\sqrt{\dfrac{2}{z}}v\left[\delta - m_1\left(v^2+w^2\right)\right] + m_2 e^{-2az^{-1}}\right), \\ \dfrac{dw}{dt} = \dfrac{1}{\sqrt{\delta}}\sqrt{\dfrac{2}{z}}w\left[\delta - m_1\left(v^2+w^2\right)\right]. \end{cases} \tag{66}$$

For any solution $(z(t), v(t), w(t))$ of (66), $(1/z(t), v(t), w(t))$ traces the corresponding solution orbit of (1) but with a different speed. Starting from

$$(z(0), v(0), w(0)) = \left(\frac{1}{1200}, -\sqrt{\frac{\delta}{m_1}} \cos\theta, \sqrt{\frac{\delta}{m_1}} \sin\theta \right),$$

we iterated the time-T map for (66) by the Taylor expansion method until both

$$v > 0 \quad \text{and} \quad (v^2 + w^2)\frac{m_1}{\delta} - 1 < \varepsilon_{\text{tol}}$$

hold for some predefined tolerance $\varepsilon_{\text{tol}} > 0$. We regard the final value of $\tan^{-1}(w/v)$ as the numerical estimate of θ_{ref}. We selected T and ε_{tol} depending on δ. For smaller δ, we should select larger T and smaller ε_{tol}. There are some parameters for numerical experiments, such as the precision of MPFR (corresponding to greater than one hundred decimal digits in some cases), error tolerance(s) for step size control, and the order of Taylor expansion.

4.3 Results of Numerical Experiments

In order to test our conjectures for κ, and hence χ, we estimated κ numerically, using the methods described above. For fixed δ, m_0, m_1, m_2, a and θ_{inc}, let us define an empirical estimate of $\kappa(m_0 m_1/\sqrt{a}, m_1^2 m_2/a^{5/2})$ by

$$\underline{\kappa}(\delta, m_0, m_1, m_2, a, \theta_{\text{inc}}) = \frac{a}{\sqrt{\delta m_1}\sin\theta_{\text{inc}}\cos^2\theta_{\text{inc}}}(\underline{\theta}_{\text{ref}} - \theta_{\text{inc}}), \tag{67}$$

where $\underline{\theta}_{\text{ref}}$ is the numerical estimate computed by numerical integration.

We computed $\underline{\kappa}(\delta, 1, 1, 1, 1, \theta_{\text{inc}})$ using the two integrators described above for $\theta_{\text{inc}} \in \{0.32, 0.62, 0.92\}$ and some values of δ in the range $[10^{-30}, 10^{-10}]$. The digits shown in Table 3 are in agreement for both integrators (and Maple). Thus, our integrators return consistent results despite their differing constructions, and their results do appear to be reliable. One also sees slow convergence: the difference between the cases $\delta = 10^{-10}$ and 10^{-30} is of order 10^{-3}. It is worth noting that this slow convergence was the primary reason why it was necessary to perform numerical calculations for extremely small values of δ to test our conjectures. Note that Table 3 also suggests that the limit of $\underline{\kappa}(\delta, 1, 1, 1, 1, \theta_{\text{inc}})$ as δ goes to zero may possibly be a rational number, since $2.6667 \approx 8/3$. It was the repeated appearance of what could be interpreted as numerical approximations of simple rational numbers which eventually led to the conjectured form of χ in (58).

With regard to the behavior of χ, which is fundamental to Conjecture 3, please refer to Figure 8.

In the following, we first show that $\kappa(\alpha, \beta)$ appears to be a linear function of α/β and then that it appears to be converging towards the specific linear function (58) appearing on the right hand side of equation (10) in our Main Conjecture.

Table 3: Reliable digits of $\underline{\kappa}(\delta, 1, 1, 1, 1, \theta_{\text{inc}})$, confirmed using multiple methods of calculation. Our Main Conjecture suggests that the limit in each column should be $8/3 \approx 2.6667$.

$\log_{10}\delta$	$\theta_{\text{inc}} = 0.32$	$\theta_{\text{inc}} = 0.62$	$\theta_{\text{inc}} = 0.92$
-10	2.667322622150928	2.667276262637233	2.667206671078424
-14	2.666990666912656	2.666984327424471	2.666972800168754
-16	2.666915082395880	2.666910981702080	2.666903404396998
-18	2.666863194397326	2.666860319298610	2.666854976727414
-20	2.666825989326286	2.666823888143940	2.666819970532292
-22	2.666798408320533	2.666796825841195	2.666793867683524
-26	2.666761035254502	2.666760073269559	2.666758267870788
-30	2.666737550541605	2.666736923025252	2.666735741891223

For selected values of δ in $[10^{-100}, 10^{-2}]$, we computed $\underline{\kappa}$ for 10,000 samples of $(m_0, m_2, a, \theta_{\text{inc}})$, uniformly distributed in $[0.1, 10] \times [0.1, 10] \times [0.25, 4] \times (0, \pi/2)$, while keeping $m_1 = 1$ (without loss of generality due to (54)). We fitted a linear function of $m_0 a^2/(m_1 m_2)$ by linear regression implemented in scikit-learn [22]. Multiple-precision arithmetic was used for computing each sample, while double-precision was used for plotting and regression.

Figure 9 presents results for $\delta = 10^{-n}$ for $n = 6, 10, 30, 100$, the fitted linear function, and the conjectured linear function (58). The empirical estimates are closer to the fitted linear function for smaller δ. We can see such behavior in Table 4, which shows the values of δ, intercepts and slopes of the fitted linear functions, and the coefficient of determination R^2 for the linear regression. These results suggest that κ is univariate in the limit $\delta \to 0$, that is, $\kappa(\alpha, \beta) = \hat{\chi}(\alpha/\beta)$ for some linear function $\hat{\chi}$.

Next, we investigated the intercept and slope of the fitted linear function $\hat{\chi}(r)$. Let $m_1 = a = 1$, making use of the identity (54) to reduce the dimension of parameter space without loss of generality. We have $r = m_0 a^2/(m_1 m_2) = m_0/m_2$. The results for $\underline{\kappa}(10^{-100}, r, 1, 1, 1, \theta_{\text{inc}})$ and $\underline{\kappa}(10^{-250}, r, 1, 1, 1, \theta_{\text{inc}})$ for $\theta_{\text{inc}} \in \{0.32, 0.62, 0.92\}$ are shown in Tables 5 and 6. These are indeed suggestive of the conjectured linear expression for χ, defined in (58).

We examined the apparent convergence towards $\chi(r)$ by computing

$$\underline{\chi}(\delta, r, \theta_{\text{inc}}) := \underline{\kappa}(\delta, r, 1, 1, 1, \theta_{\text{inc}}). \tag{68}$$

For actual values, see Tables 7 to 11. Figure 10 shows plots of $|\underline{\chi}(\delta, r, \theta_{\text{inc}}) - \chi(r)|$ with respect to δ. It behaves like $1/(\log_{10}\delta)^2$ for $r = 1$ and $1/|\log_{10}\delta|$ for $r = 0, 0.5, 1.5, 2$.

In order to understand whether this is due to the ratio m_0/m_2 or the choice of $m_2 = 1$ (with $m_0 = r$), additional experiments were performed for $\underline{\kappa}(\delta, 2, 1, 2, 1, \theta_{\text{inc}})$ and $\underline{\kappa}(\delta, 1/2, 1, 1/2, 1, \theta_{\text{inc}})$, giving the same conclusion as for $m_0 = m_2 = 1$ (i.e. $r = 1$). For $r = 0$, $r = 1/2$, $r = 3/2$ and $r = 2$, additional experiments were performed for $\underline{\kappa}(\delta, 0, 1, 2, 1, \theta_{\text{inc}})$ and $\underline{\kappa}(\delta, 0, 1, 1/2, 1, \theta_{\text{inc}})$, $\underline{\kappa}(\delta, 1, 1, 2, 1, \theta_{\text{inc}})$,

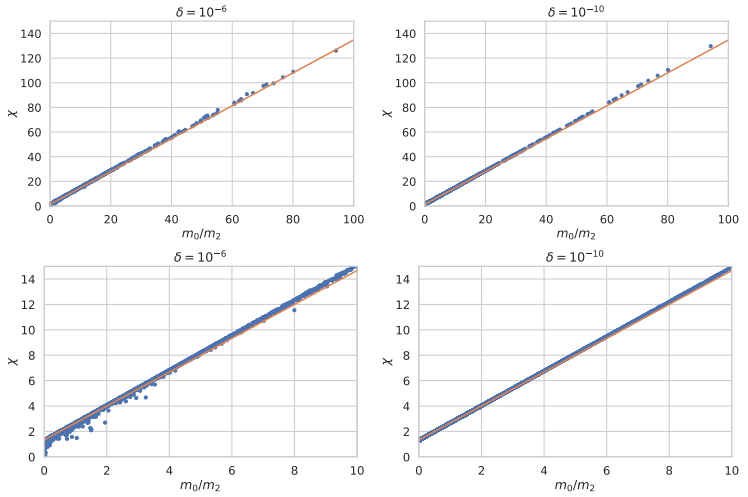

Figure 8: Detailed illustration of the conjectured identity (56). Numerical integration of (1) with $\delta = 10^{-6}$ (left side) and $\delta = 10^{-10}$ (right side), and $m_1 = a = 1$ (no loss of generality due to (54)) was performed for 10,000 randomly chosen parameter sets (m_0, m_2) in $[0.1, 10]^2$. Comparing left to right, the empirical values of κ appear to be converging towards a function of m_0/m_2 (i.e. $\chi(m_0/m_2)$) as δ decreases.

$\underline{\kappa}(\delta, 3, 1, 2, 1, \theta_{\text{inc}})$, and $\underline{\kappa}(\delta, 1, 1, 0.5, 1, \theta_{\text{inc}})$, respectively, all confirming the behavior seen for $\underline{\chi}(\delta, r, \theta_{\text{inc}})$.

In total, these experiments support the conjecture that $|\underline{\chi}(\delta, r, \theta_{\text{inc}}) - \chi(r)|$ behaves as $1/(\log_{10}\delta)^2$ for $m_0/m_2 = 1$ and $1/|\log_{10}\delta|$ for $m_0/m_2 = 0, 0.5, 1.5, 2$. The convergence is slower than polynomial, and yet $\underline{\kappa}(\delta, m_0, 1, m_2, 1, \theta_{\text{inc}}) \to (4/3)(1 + m_0/m_2)$ as $\delta \to 0$ certainly does appear to hold.

Our experiments seem to allow one to speculate that, as $\delta \to 0^+$,

$$\theta_{\text{ref}} = \theta_{\text{inc}} + \frac{4}{3}\left(1 + \frac{m_0 a^2}{m_1 m_2}\right)\frac{\sqrt{\delta m_1}}{a}\sin\theta_{\text{inc}}\cos^2\theta_{\text{inc}} + O\left(\frac{\sqrt{\delta}}{|\ln\delta|}\right), \tag{69}$$

however, clarifying more precisely the nature of the error term would be beyond the scope of our current investigation, partly because it would likely depend upon our specific choice of the interaction function h_a. Our primary aim here remains the investigation of what is likely to be common to all such models.

The combined outcome of our experiments (including all of those not reported here) is that our Main Conjecture is supported numerically.

5 Concluding remarks

We studied a particle model composed of ordinary differential equations derived from a planar reaction-diffusion model of a camphor disk on the surface of water

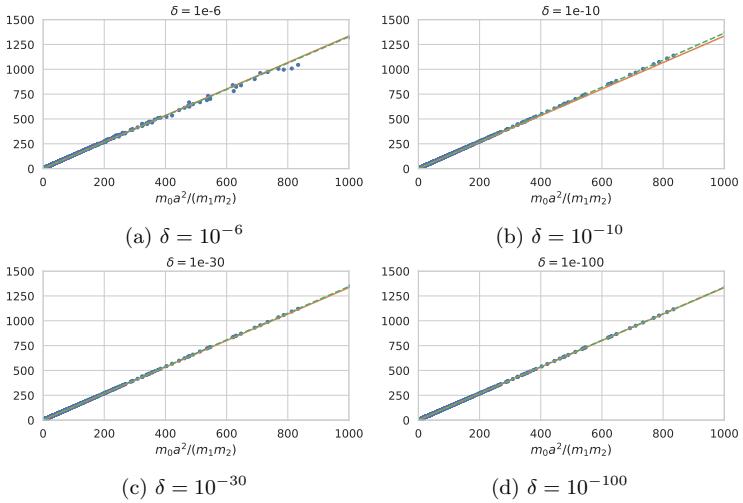

(a) $\delta = 10^{-6}$ (b) $\delta = 10^{-10}$

(c) $\delta = 10^{-30}$ (d) $\delta = 10^{-100}$

Figure 9: Plots of $\underline{\kappa}(\delta, m_0, 1, m_2, a, \theta_{\text{inc}})$ (vertical axes) against $m_0a^2/(m_1m_2)$. The solid line is the conjectured limit $(4/3)(1 + m_0a^2/(m_1m_2))$ (equation (58)), and the dashed line was fitted by linear regression.

[3]. The model system of ordinary differential equations is not Hamiltonian, and, for a particle reflecting from a single linear boundary, the exact relationship between the angle of reflection and the angle of incidence is not known, although several of its properties have been revealed in previous work, such as the fact that the angle of reflection must be greater than the angle of incidence [5].

Here, we have been able to experimentally identify a general asymptotic expression for the angle of reflection as a function of the angle of incidence, in the limit of small δ, which can be understood as a low speed limit. It has not been necessary to restrict the values of model parameters.

Our conjecture is of importance since the system (1) in the limit of small δ represents universal properties of planar reaction-diffusion system particle dynamics.

Acknowledgements

This work was supported by JSPS KAKENHI Grant Number 19K03626 and MEXT Promotion of Distinctive Joint Research Center Program Grant Number JPMXP0620335886.

Statements and declarations

The authors report there are no competing interests to declare.

Table 4: Line fitting of empirical estimates of $\kappa(\alpha, \beta)$ to a linear function $\hat{\chi}(\alpha/\beta)$ by linear regression. The conjectured linear function χ, defined by (58), has an intercept of $4/3 \approx 1.33$ and a slope of $4/3 \approx 1.33$.

$\log_{10} \delta$	intercept	slope	R^2
-2	8.468996367394844	0.4337314440471723	0.3385515789325083
-3	7.1530211906893335	0.692490027395997	0.7401348661198679
-4	4.723522841674198	1.0060248805116885	0.9395812998171977
-5	2.7120013519151343	1.2282488639523028	0.9912569147805238
-6	1.7707959781907618	1.3254754000572635	0.998994314520452
-8	1.3198559208767229	1.3653480685814732	0.9999879664914185
-10	1.2874448621912222	1.3630795035390868	0.9999969425823786
-20	1.3130545968418694	1.3482371520102885	0.9999997528123326
-30	1.3210754895334773	1.3431966907454091	0.9999999485410582
-40	1.3246180894269592	1.3407006200830112	0.9999999832564618
-50	1.3265920921196361	1.3392114708372023	0.9999999930217386
-100	1.3301953617468243	1.3362546221487297	0.9999999995458777

Table 5: Computed values of $\underline{\kappa}(\delta, r, 1, 1, 1, \theta_{\text{inc}})$ for $\delta = 10^{-100}$, rounded to 8 decimal places. The conjectured (according to (58)) values of χ would be $4/3 \approx 1.33333$ for $r = 0.0$, 2 for $r = 0.5$, $8/3 \approx 2.66667$ for $r = 1.0$, $10/3 \approx 3.33333$ for $r = 1.5$ and 4 for $r = 2.0$.

r	$\theta_{\text{inc}} = 0.02$	0.32	0.62	0.92	1.22
0.0	1.33042613	1.33042745	1.33043133	1.33043875	1.33045290
0.5	1.99854958	1.99855023	1.99855216	1.99855586	1.99856290
1.0	2.66667302	2.66667301	2.66667300	2.66667296	2.66667290
1.5	3.33479646	3.33479580	3.33479383	3.33479007	3.33478290
2.0	4.00291991	4.00291858	4.00291466	4.00290718	4.00289290

References

[1] Bengtsson, L., Böttger, H., Kanamitsu, M.: Simulation of hurricane-type vortices in a general circulation model. Tellus **34**:5 440–457 (1982)

[2] Boniface, D., Cottin-Bizonne, C., Kervil, R., Ybert, C., Detcheverry, F.: Self-propulsion of symmetric chemically active particles: Point-source model and experiments on camphor disks. Phys. Rev. E **99**:6 062605 (2019)

[3] Chen, X., Ei, S.-I., Mimura, M.: Self-motion of camphor discs. model and analysis. Netw. Heterog. Media **4** 1–18 (2009)

[4] De Buyl, P., Mikhailov, A.S., Kapral, R.: Self-propulsion through symmetry breaking. Europhysics Letters **103**:6 60009 (2013)

Table 6: Computed values of $\underline{\kappa}(\delta, r, 1, 1, 1, \theta_{\mathrm{inc}})$ for $\delta = 10^{-250}$, rounded to 8 decimal places. The conjectured (according to (58)) values of χ would be $4/3 \approx 1.33333$ for $r = 0.0$, 2 for $r = 0.5$, $8/3 \approx 2.66667$ for $r = 1.0$, $10/3 \approx 3.33333$ for $r = 1.5$ and 4 for $r = 2.0$.

r	$\theta_{\mathrm{inc}} = 0.02$	0.32	0.62	0.92	1.22
0.0	1.33217239	1.33217260	1.33217323	1.33217442	1.33217669
0.5	1.99942004	1.99942014	1.99942045	1.99942105	1.99942218
1.0	2.66666768	2.66666768	2.66666768	2.66666767	2.66666767
1.5	3.33391532	3.33391521	3.33391490	3.33391430	3.33391316
2.0	4.00116296	4.00116275	4.00116213	4.00116093	4.00115865

Table 7: Computed values of $\underline{\chi}(\delta, 1, \theta_{\mathrm{inc}})$, rounded to 8 decimal places. The conjectured (according to (58)) value of $\chi(1)$ would be $8/3 \approx 2.666667$.

$\log_{10} \delta$	$\theta_{\mathrm{inc}} = 0.02$	0.32	0.62	0.92	1.22
-10	2.66734088	2.66732262	2.66727626	2.66720667	2.66709257
-14	2.66699287	2.66699067	2.66698433	2.66697280	2.66695237
-16	2.66691649	2.66691508	2.66691098	2.66690340	2.66688981
-18	2.66686418	2.66686319	2.66686032	2.66685498	2.66684532
-20	2.66682671	2.66682599	2.66682389	2.66681997	2.66681285
-22	2.66679895	2.66679841	2.66679683	2.66679387	2.66678846
-30	2.66673776	2.66673755	2.66673692	2.66673574	2.66673356
-40	2.66670660	2.66670651	2.66670625	2.66670575	2.66670481
-50	2.66669219	2.66669215	2.66669201	2.66669175	2.66669127
-100	2.66667302	2.66667301	2.66667300	2.66667296	2.66667290
-150	2.66666948	2.66666948	2.66666948	2.66666947	2.66666945
-200	2.66666825	2.66666825	2.66666825	2.66666824	2.66666823
-250	2.66666768	2.66666768	2.66666768	2.66666767	2.66666767

[5] Ei, S.-I., Mimura, M., Miyaji, T.: Reflection of a self-propelling rigid disk from a boundary. Discrete Contin. Dyn. Syst. S **14**:3 803–817 (2021)

[6] Ei, S.-I., Mimura, M., Nagayama, M.: Interacting spots in reaction diffusion systems. Discrete Contin. Dyn. Syst. **14** 31–62 (2006)

[7] Fousse, L., Hanrot, G., Lefèvre, V., Pélissier, P., Zimmermann, P.: MPFR: A multiple-precision binary floating-point library with correct rounding. ACM Transactions on Mathematical Software **33**:2 Article 13 (2007) `https://www.mpfr.org` Accessed 04 July 2022

[8] Garwin, R.L.: Kinematics of an Ultraelastic Rough Ball. American Journal of Physics **37**:1 88–92 (1969)

Table 8: Computed values of $\underline{\chi}(\delta, 0, \theta_{\text{inc}})$, rounded to 8 decimal places. The conjectured (according to (58)) value of $\chi(0)$ would be $4/3 \approx 1.333$.

$\log_{10}\delta$	$\theta_{\text{inc}} = 0.02$	0.32	0.62	0.92	1.22
−10	1.30457185	1.30469208	1.30504369	1.30569567	1.30685407
−14	1.31265468	1.31272006	1.31291147	1.31326908	1.31392196
−16	1.31520923	1.31525958	1.31540725	1.31568399	1.31619231
−18	1.31720459	1.31724454	1.31736181	1.31758216	1.31798880
−20	1.31880586	1.31883831	1.31893367	1.31911320	1.31944579
−22	1.32011903	1.32014591	1.32022496	1.32037403	1.32065105
−30	1.32363262	1.32364714	1.32368996	1.32377107	1.32392308
−40	1.32605614	1.32606433	1.32608851	1.32613446	1.32622110
−50	1.32751232	1.32751757	1.32753307	1.32756259	1.32761845
−100	1.33042613	1.33042745	1.33043133	1.33043875	1.33045290
−150	1.33139672	1.33139730	1.33139903	1.33140233	1.33140865
−200	1.33188163	1.33188196	1.33188293	1.33188478	1.33188834
−250	1.33217239	1.33217260	1.33217323	1.33217442	1.33217669

[9] Gérardin, B., Laurent, J., Ambichl, P., Prada, C., Rotter, S., Aubry, A.: Particlelike wave packets in complex scattering systems. Phys. Rev. B **94**:1 014209 (2016)

[10] Kitahata, H., and Yoshikawa, K.: Chemo-mechanical energy transduction through interfacial instability. Phys. D **205** 283–291 (2005)

[11] Krischer, K., Mikhailov, A.: Bifurcation to Traveling Spots in Reaction-Diffusion Systems. Phys. Rev. Lett. **73**:23 3165–3168 (1994)

[12] Langham, J., Barkley, D.: Non-specular reflections in a macroscopic system with wave-particle duality: Spiral waves in bounded media. Chaos **23** 013134 (2013)

[13] Langham, J., Biktasheva, I., Barkley, D.: Asymptotic dynamics of reflecting spiral waves. Phys. Rev. E **90** 062902 (2014)

[14] Lorenz, E.N.: Deterministic Nonperiodic Flow. Journal of the Atmospheric Sciences **20**:2 130–141 (1963)

[15] Maple (2019.2). Maplesoft, a division of Waterloo Maple Inc., Waterloo, Ontario. `https://www.maplesoft.com/products/Maple/` Accessed 04 July 2022

[16] Mimura, M., Miyaji, T., Ohnishi, I.: A billiard problem in nonlinear and nonequilibrium systems. Hiroshima Math. J. **37** 343–384 (2007)

[17] Miyaji, T.: Arnold tongues in a billiard problem in nonlinear and nonequilibrium systems. Phys. D **340** 14–25 (2017)

Table 9: Computed values of $\underline{\chi}(\delta, 1/2, \theta_{\mathrm{inc}})$, rounded to 8 decimal places. The conjectured (according to (58)) value of $\chi(1/2)$ would be 2.

$\log_{10}\delta$	$\theta_{\mathrm{inc}} = 0.02$	0.32	0.62	0.92	1.22
−10	1.98595637	1.98600779	1.98616125	1.98645295	1.98697473
−14	1.98982377	1.98985537	1.98994791	1.99012096	1.99043718
−16	1.99106286	1.99108733	1.99115912	1.99129370	1.99154106
−18	1.99203438	1.99205387	1.99211107	1.99221857	1.99241706
−20	1.99281628	1.99283215	1.99287878	1.99296659	1.99312932
−22	1.99345899	1.99347216	1.99351089	1.99358395	1.99371976
−30	1.99518519	1.99519235	1.99521344	1.99525340	1.99532832
−40	1.99638137	1.99638542	1.99639738	1.99642010	1.99646295
−50	1.99710226	1.99710486	1.99711254	1.99712717	1.99715486
−100	1.99854958	1.99855023	1.99855216	1.99855586	1.99856290
−150	1.99903310	1.99903339	1.99903425	1.99903590	1.99903905
−200	1.99927494	1.99927510	1.99927559	1.99927651	1.99927829
−250	1.99942004	1.99942014	1.99942045	1.99942105	1.99942218

[18] Nakata, S., Nagayama, M.: Chapter 1: Theoretical and Experimental Design of Self-propelled Objects Based on Nonlinearity. In Self-organized Motion: Physicochemical Design based on Nonlinear Dynamics, S. Nakata et al.(eds), 1–30 (2019)

[19] Nishiura, Y.: Far-from-Equilibrium Dynamics. translated by K. Sakamoto, American Mathematical Society, Providence, Rhode Island (2002)

[20] Nishiura, Y., Teramoto, T.: Refraction, Reflection and Splitting. RIMS Kôkyûroku Bessatsu **B31** 167–194 (2012)

[21] Olmos, D., Shizgal, B.: Annihilation and reflection of spiral waves at a boundary for the Beeler-Reuter model. Phys. Rev. E **77** 031918 (2008)

[22] Pedregosa, F., Varoquaux, G., Gramfort, A., Michel, V., Thirion, B., Grisel, O., Blondel, M., Prettenhofer, P., Weiss, R., Dubourg, V., Vanderplas, J., Passos, A., Cournapeau, D., Brucher, M., Perrot, M., Duchesnay, E.: Scikit-learn: Machine Learning in Python. Journal of Machine Learning Research **12** 2825–2830 (2011)

[23] Prati, F., Lugiato, L.A., Tissoni, G., Brambilla, M.: Cavity soliton billiards. Phys. Rev. A **84** 053852 (2011)

[24] Protière, S., Boudaoud, A., Couder, Y.: Particle-wave association on a fluid interface. Journal of Fluid Mechanics **554** 85–108 (2006)

[25] Pucci, G., Sáenz, P.J., Faria, L.M., Bush, J.W.M.: Non-specular reflection of walking droplets. Journal of Fluid Mechanics **804** R3 (2016)

Table 10: Computed values of $\underline{\chi}(\delta, 3/2, \theta_{\text{inc}})$, rounded to 8 decimal places. The conjectured (according to (58)) value of $\chi(3/2)$ would be $10/3 \approx 3.33333$.

$\log_{10}\delta$	$\theta_{\text{inc}} = 0.02$	0.32	0.62	0.92	1.22
−10	3.34872537	3.34863657	3.34838872	3.34795683	3.34720761
−14	3.34416196	3.34412596	3.34402072	3.34382461	3.34346753
−16	3.34277012	3.34274283	3.34266285	3.34251311	3.34223855
−18	3.34169397	3.34167252	3.34160957	3.34149139	3.34127358
−20	3.34083713	3.34081983	3.34076900	3.34067335	3.34049637
−22	3.34013891	3.34012466	3.34008276	3.34000379	3.33985717
−30	3.33829034	3.33828275	3.33826041	3.33821808	3.33813879
−40	3.33703184	3.33702760	3.33701512	3.33699139	3.33694666
−50	3.33628213	3.33627943	3.33627148	3.33625633	3.33622768
−100	3.33479646	3.33479580	3.33479383	3.33479007	3.33478290
−150	3.33430586	3.33430557	3.33430470	3.33430303	3.33429985
−200	3.33406156	3.33406139	3.33406091	3.33405997	3.33405818
−250	3.33391532	3.33391521	3.33391490	3.33391430	3.33391316

[26] Suematsu, N.J., Nakata, S.: Evolution of self-propelled objects: From the viewpoint of nonlinear science. Chemistry – A European Journal **24** 6308–6324 (2018)

[27] Teramoto, T., Suzuki, K., Nishiura, Y.: Rotational motion of traveling spots in dissipative systems. Phys. Rev. E **80** 046208 (2009)

[28] Tlidi, M., Staliunas, K., Panajotov, K., Vladimirov, A.G., Clerc, M.G.: Localized structures in dissipative media: from optics to plant ecology. Phil. Trans. R. Soc. A. **372** 20140101 (2014)

[29] Uspal, W.E., Popescu, M.N., Dietrichab, S., Tasinkevych, M.: Self-propulsion of a catalytically active particle near a planar wall: from reflection to sliding and hovering. Soft Matter **11** 434–438 (2015)

[30] Verner, J.H.: Explicit Runge-Kutta Methods with Estimates of the Local Truncation Error. SIAM Journal on Numerical Analysis **15**:4 772–790 (1978)

[31] Wilczak, D.: The CAPD group. `http://capd.sourceforge.net/capdDynSys/` Accessed 04 July 2022

[32] Winfree, A.T.: Spiral waves of chemical activity. *Science* **175**:4022 634–636 (1972)

Table 11: Computed values of $\underline{\chi}(\delta, 2, \theta_{\text{inc}})$, rounded to 8 decimal places. The conjectured (according to (58)) value of $\chi(2)$ would be 4.

$\log_{10}\delta$	$\theta_{\text{inc}} = 0.02$	0.32	0.62	0.92	1.22
−10	4.03010986	4.02994964	4.02949862	4.02870343	4.02731985
−14	4.02133106	4.02126124	4.02105708	4.02067638	4.01998267
−16	4.01862376	4.01857058	4.01841471	4.01812280	4.01758729
−18	4.01652377	4.01648185	4.01635883	4.01612779	4.01570184
−20	4.01484756	4.01481367	4.01471411	4.01452674	4.01417990
−22	4.01347886	4.01345090	4.01336869	4.01321371	4.01292587
−30	4.00984291	4.00982796	4.00978389	4.00970042	4.00954403
−40	4.00735707	4.00734869	4.00732399	4.00727703	4.00718852
−50	4.00587206	4.00586672	4.00585095	4.00582091	4.00576408
−100	4.00291991	4.00291858	4.00291466	4.00290718	4.00289290
−150	4.00194225	4.00194166	4.00193992	4.00193660	4.00193025
−200	4.00145487	4.00145454	4.00145357	4.00145170	4.00144813
−250	4.00116296	4.00116275	4.00116213	4.00116093	4.00115865

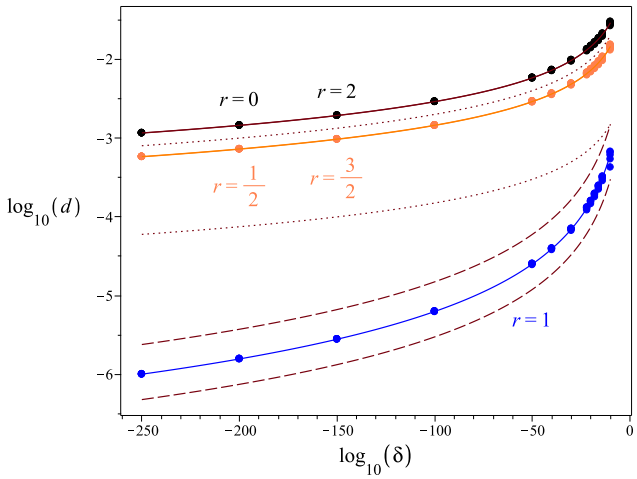

Figure 10: The difference $d = |\underline{\chi}(\delta, r, \theta_{\text{inc}}) - \chi(r)|$ plotted against δ for $\theta_{\text{inc}} \in \{0.02, 0.04, \ldots 1.22\}$. The dotted curves are proportional to $1/|\ln\delta|$, and the dashed curves proportional to $1/|\ln\delta|^2$.